



## Search for high- $T_C$ conventional superconductivity at megabar pressures in the lithium-sulfur system

Christian Kokail,<sup>1</sup> Christoph Heil,<sup>2</sup> and Lilia Boeri<sup>1</sup>

<sup>1</sup>*Institute of Theoretical and Computational Physics, Graz University of Technology, NAWI Graz, 8010 Graz, Austria*

<sup>2</sup>*Department of Materials, University of Oxford, Parks Road, Oxford OX1 3PH, United Kingdom*

(Received 24 May 2016; published 1 August 2016)

Motivated by the recent report of superconductivity above 200 K in ultra-dense hydrogen sulfide, we search for high- $T_C$  conventional superconductivity in the phase diagram of the binary Li-S system, using *ab initio* methods for crystal structure prediction and linear response calculations for the electron-phonon coupling. We find that at pressures higher than 20 GPa, several new compositions, besides the known  $\text{Li}_2\text{S}$ , are stabilized; many exhibit electrone-like *interstitial* charge localization observed in other alkali-metal compounds. Of all predicted phases, only an fcc phase of  $\text{Li}_3\text{S}$ , metastable before 640 GPa, exhibits a sizable  $T_C$ , in contrast to what is observed in sulfur and phosphorus hydrides, where several stoichiometries lead to high  $T_C$ . We attribute this difference to  $2s$ - $2p$  hybridization and avoided core overlap, and predict similar behavior for other alkali-metal compounds.

DOI: [10.1103/PhysRevB.94.060502](https://doi.org/10.1103/PhysRevB.94.060502)

The successful prediction of a record critical temperature ( $T_C$ ) of 203 K in hydrogen sulfide ( $\text{H}_3\text{S}$ ) at 200 GPa [1–3] gave a considerable impulse to the *ab initio* design of new high- $T_C$  superconductors at extreme pressures.  $\text{H}_3\text{S}$  was in fact the first example of a *conventional* high-temperature superconductor whose crystal structure and  $T_C$  were first predicted completely from first principles and later confirmed experimentally. It is now understood that its record-high  $T_C$  stems from the constructive interference of large vibrational frequencies, electronic van-Hove singularities at the Fermi level, and large electron-phonon ( $ep$ ) matrix elements due to the formation of *covalent* H-S bonds [3–11]. A few months after the  $\text{H}_3\text{S}$  discovery, a high- $T_C$  superconducting phase was also found in compressed phosphines, which is compatible with several *metastable*  $\text{PH}_x$  phases identified by first-principles calculations [12–15]. Recent reports of metallization in hydrogen at  $\sim 350$  GPa have given rise to the hope of attaining superconductivity at room temperatures or even higher [16–22]. While several hydrides have been proposed as prospective superconductors along the lines of  $\text{H}_3\text{S}$  [23–28], high- $T_C$  superconductivity at high pressures in hydrogen-free compounds is still a largely unexplored field.

In this work we search for high- $T_C$  superconductivity at extreme pressures in the Li-S system, using the USPEX method for *ab initio* evolutionary crystal structure prediction [29] and density functional perturbation theory (DFPT) calculations of the  $ep$  coupling as implemented in the QUANTUM ESPRESSO code [30,31]. The underlying idea is to explore a hydrogen-free system similar to  $\text{H}_3\text{S}$ ; Li-S is a natural choice, because lithium belongs to the same group as hydrogen (similar chemical properties) and has a small atomic mass (large phonon frequencies). At ambient pressure, Li-S is stable in crystalline form in the  $\text{Li}_2\text{S}$  composition; this compound has applications in lithium-based batteries, and has been investigated by several authors [32,33]. We find that at high pressures several new phases are stabilized, many of which behave quite differently from the corresponding hydrides; in particular, superconductivity is harder to attain, and the typical  $T_C$ 's are much lower. We will show that this can be explained by the different chemistry of the two elements, caused by the presence or absence of core electrons [34].

In fact, lithium passes through a sequence of transitions under pressure from close-packed, metallic structures to open, semimetallic or semiconducting ones [35–38]. The increasing covalency is induced by the growing  $2s$ - $2p$  hybridization and is accompanied by the characteristic phenomenon of *interstitial charge localization*; i.e., the electronic valence charge tends to localize in interstitial regions of the crystal to minimize the overlap with underlying atomic core states (*avoided core overlap*) [38–42]. Hydrogen, whose  $1s$  valence electrons have no underlying core and are well separated in energy from  $2p$  states, has a completely different behavior, transforming from molecular insulating to close-packed metallic structures at very high pressures [43]. The highest  $T_C$ 's in the two elements range from  $\sim 16$  K, measured in lithium at 100 GPa [44,45], to  $\sim 350$  K predicted for hydrogen in the metallic phase [16–19].

Figure 1 shows our theoretical phase diagram for the Li-S system, constructed with a four-step procedure. (i) First, we performed a preliminary scan of the phase space, with variable-composition evolutionary algorithm (EA) runs from 0 to 600 GPa at 50-GPa intervals. (ii) For the most promising phases, i.e., those that lie on the convex hull, we ran additional calculations at fixed compositions with 100-GPa intervals starting from 0 GPa to identify thermodynamically stable phases. (iii) The best three structures from each fixed composition run were relaxed once more with stricter convergence parameters to ensure the correct enthalpy hierarchy of the phases. (iv) The best individuals were relaxed further with a tighter convergence threshold, at pressure intervals of 50–100 GPa, and the resulting energy vs volume curves were then fitted to a Murnaghan equation of state [46]. This allowed us to obtain analytical expressions for the enthalpy vs pressure relation for all structures, from which we could extract accurate stability ranges for all phases [47,48]. Note that in order to maintain our search within a reasonable time limit, we restricted the search space to phases with a maximum of 24 atoms per unit cell and 6 atoms per formula unit (f.u.).

Before discussing the new phases found in our EA search, we note that our calculations reproduce accurately literature results for the known phases, that is, for the two end members and  $\text{Li}_2\text{S}$ . For elemental lithium, we find essentially the same phase diagram as in Ref. [49], i.e., we predict a transition from

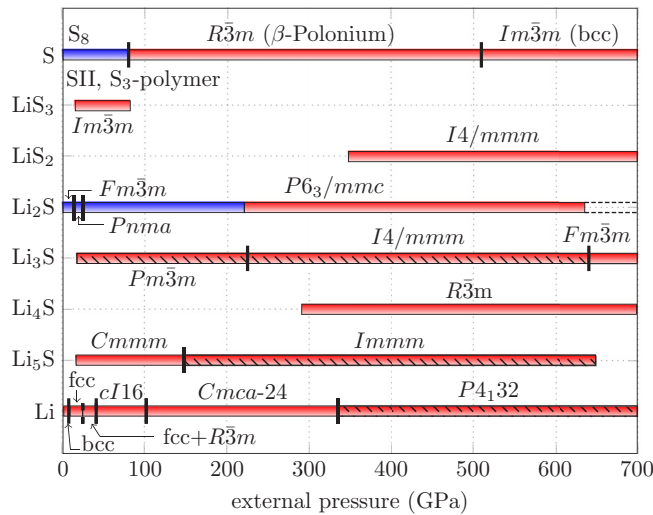


FIG. 1. Phase diagram for the Li-S system predicted by our DFT-EA search. The vertical bars delimit regions of stability. Blue and red bars indicate insulating and metallic phases, respectively. Shaded areas indicate phases with interstitial charge localization (see text).

a *bcc* to an *fcc* phase and then into a *cI16* phase, stable until 100 GPa [35]. At 100 GPa, a *Cmca* phase with 24 atoms is stabilized and remains the lowest in enthalpy up to  $\sim 330$  GPa, where a simple cubic (*P4<sub>1</sub>32*) phase occurs. Our results are in very good agreement with previous works which employ unit cells up to 24 atoms [36,37], while recent calculations with larger supercells predicted two additional phases between 60 and 270 GPa: *Aba2-40* (40 atoms per cell) and *Cmca-56* (56 atoms per cell). Having verified that the enthalpy differences with respect to the *Cmca-24* phases are minimal and do not affect the calculated convex hull, we decided to use the *Cmca-24* phase in the whole range. For sulfur, we predict a transition from the S<sub>8</sub>  $\alpha$  phase to the polymeric S-II (2 GPa) and S<sub>3</sub>-polymer (20 GPa) phases [50]. At 80 GPa, the S<sub>3</sub>-polymer phase transforms into the  $\beta$ -Po phase, which is metallic. At very large pressures ( $\sim 510$  GPa) we predict a transition to a standard *bcc* phase, as in Ref. [51]. In agreement with previous calculations, and despite several attempts, we did not find any indication of a *bco* phase as seen by experiments between 83 and 162 GPa [52]. For Li<sub>2</sub>S, we correctly predict a transition from the antifluorite structure (*Fm̄3m*) at ambient pressure to the anticotunnite structure at 13 GPa. At pressures higher than 26 GPa, a Ni<sub>2</sub>In-type structure (*P6<sub>3</sub>/mmc*), shown in Fig. 2, becomes stable; similar transition sequences are observed in other alkali-metal sulfides as Na<sub>2</sub>S and K<sub>2</sub>S [53,54], as well as in the closely related compound Li<sub>2</sub>O. [33] The *P6<sub>3</sub>/mmc* phase remains insulating up to 221 GPa, where an insulator-to-metal transition takes place; we find that this phase remains stable up to the highest pressure we calculated.

For pressures higher than 20 GPa, several new compositions are stabilized; the relative structures are detailed in the Supplemental Material (SM) [55] together with band structure plots and results of DFPT calculations. Figure 2 only shows those relevant to our discussion, decorated with isosurfaces of the electronic localization function (ELF). We start the discussion from the Li-rich side: The Li<sub>5</sub>S composition becomes stable at

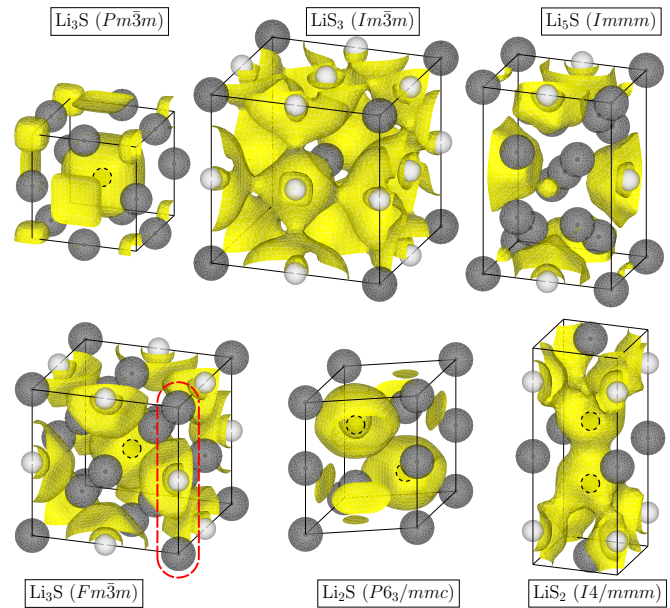


FIG. 2. Crystal structure and isocontour (0.65) of the ELF for (top) Li<sub>3</sub>S-*Pm̄3m* (100 GPa), LiS<sub>3</sub>-*Im̄3m* (100 GPa), and Li<sub>5</sub>S-*Immm* (500 GPa), and (bottom) Li<sub>3</sub>S-*Fm̄3m* (500 GPa), Li<sub>2</sub>S-*P6<sub>3</sub>/mmc* (500 GPa), and LiS<sub>2</sub>-*I4/mmm* (500 GPa). The structures are shown in scale; Li and S atoms are shown as black and white spheres, respectively. Black dashed circles indicate the location of S hidden by isosurfaces; red dashed lines indicate important bonds (see text).

15 GPa, in an orthorhombic *Cmmm* structure, with 12 atoms in the unit cell. This is a very open and weakly metallic structure. At  $\sim 130$  GPa, Li<sub>5</sub>S transforms to a more densely packed *Immm* phase, shown in the first row of Fig. 2. The new phase shows signatures of interstitial charge localization around the center of the tetragonal faces. The Li<sub>4</sub>S stoichiometry is stabilized only at extreme pressures ( $P > 290$  GPa); the lowest enthalpy structure is trigonal, with 10 atoms in the unit cell. Due to the low symmetry and poorly metallic behavior, we do not investigate this structure any further, but keep it in the convex hull because it has a strong influence on the stability of other phases.

Li<sub>3</sub>S is of particular interest, because it has the same stoichiometry as high-*T<sub>C</sub>* H<sub>3</sub>S. Its stability ranges from 20 GPa up to the highest pressure investigated. The lowest enthalpy structure at 20 GPa, shown in the top left corner of Fig. 2, has *Pm̄3m* space group. Sulfur occupies the *1b* positions at the center of the cube, and lithium the *3d* positions at the middle of the edges. Around the cube corners, there are large regions of empty space; the ELF isocontours show that a substantial fraction of charge tends to localize in these regions. Above 220 GPa, the simple cubic structure is destabilized toward an *I4/mmm* variant, with three f.u. in the unit cell, in which three cubic cells are stacked along one of the cubic axes, with a small in-plane mismatch. Except for the different stacking, the interatomic distances and interstitial charge localization are very similar to the *Pm̄3m* phase. At 640 GPa, the simple cubic arrangement is finally destabilized toward a completely different phase, with space group *Fm̄3m*, shown in the bottom left corner of Fig. 2. This structure, which has been reported at high

pressures for  $\text{Li}_3\text{N}$  [56], is very closely packed; it appears in our evolutionary runs already at 500 GPa and is dynamically stable up to the highest pressure we investigated. In this case, the ELF shows that the valence charge, which can no longer occupy the interstitial regions, rearranges and Li forms strong bonds with its second nearest neighbor S along the (100) direction, indicated by the red dashed line in Fig. 2. As we will show in the following, the suppression of interstitial charge localization in  $Fm\bar{3}m$ - $\text{Li}_3\text{S}$  is the reason this structure is the only high- $T_c$  superconducting phase of our study. The two S-rich phases ( $\text{LiS}_2$  and  $\text{LiS}_3$ ) have very different structures and stability ranges.  $\text{LiS}_3$  crystallizes in the same  $Im\bar{3}m$  structure as  $\text{H}_3\text{S}$ , with S occupying the  $6b$  Wyckoff positions of hydrogen, and Li the  $2a$  of S; this phase, shown in the middle of the first row in Fig. 2, is thermodynamically stable only between 20 and 80 GPa.  $\text{LiS}_2$  crystallizes in an  $I4/mmm$  crystal structure, with two f.u. (middle of lower row in Fig. 2), which is metallic and lies on the convex hull at pressures larger than 350 GPa. Both phases are superconducting with moderate  $T_c$ 's.

Our precedent study shows that there are fundamentally three pressure regimes in the high-pressure phase diagram of the Li-S system in Fig. 1: (i) a low-pressure regime ( $P < 15$  GPa), where  $\text{Li}_2\text{S}$  is the only stable composition; (ii) an intermediate regime ( $P < 200$  GPa), where new stoichiometries are stabilized; some of the new phases, such as  $\text{LiS}_3$ , disappear at higher pressures, while others remain; and (iii) a high-pressure regime, where new phases appear again. With the exception of  $\text{Li}_2\text{S}$  below 221 GPa, we identified all new phases as metallic, which leaves us with an extremely large pool of potential high- $T_c$  conventional superconductors.

For a given crystal structure and chemical composition, the superconducting  $T_c$  due to  $ep$  interaction can be estimated through the McMillan-Allen-Dynes formula

$$T_c = \frac{\omega_{\log}}{1.2k_B} \exp\left[-\frac{1.04(1+\lambda)}{\lambda - \mu^*(1+0.62\lambda)}\right]. \quad (1)$$

Here,  $k_B$  is the Boltzmann constant and  $\mu^*$  is the Coulomb pseudopotential. The  $ep$  coupling constant  $\lambda$  and the logarithmic average phonon frequency  $\omega_{\log}$  are obtained from the Eliashberg spectral function for the  $ep$  interaction  $\alpha^2F(\omega)$ , calculated within DFPT [30]

$$\alpha^2F(\omega) = \frac{1}{N(E_F)} \sum_{\mathbf{k}, \mathbf{q}, \nu} |g_{\mathbf{k}, \mathbf{k}+\mathbf{q}, \nu}|^2 \delta(\epsilon_{\mathbf{k}}) \delta(\epsilon_{\mathbf{k}+\mathbf{q}}) \delta(\omega - \omega_{\mathbf{q}, \nu}), \quad (2)$$

as  $\lambda = 2 \int d\omega \frac{\alpha^2F(\omega)}{\omega}$ ;  $\omega_{\log} = \exp\left[\frac{2}{\lambda} \int \frac{d\omega}{\omega} \alpha^2F(\omega) \ln(\omega)\right]$ . In Eq. 2,  $N(E_F)$  is the density of states (DOS) at the Fermi level,  $\omega_{\mathbf{q}, \nu}$  is the phonon frequency of mode  $\nu$  and wave vector  $\mathbf{q}$ , and  $|g_{\mathbf{k}, \mathbf{k}+\mathbf{q}, \nu}|$  is the electron-phonon matrix element between two electronic states with momenta  $\mathbf{k}$  and  $\mathbf{k} + \mathbf{q}$  at the Fermi level [57,58].

Since  $ep$  coupling calculations in DFPT are computationally much more demanding than electronic structure calculations, we could not afford a full scan of the phase space at all pressures and compositions. Instead, we selected two pressures, 100 and 500 GPa, representative of the intermediate- and high-pressure regimes, respectively, and performed  $T_c$  calculations for all phases which are stable at these pressures or in their immediate vicinity.

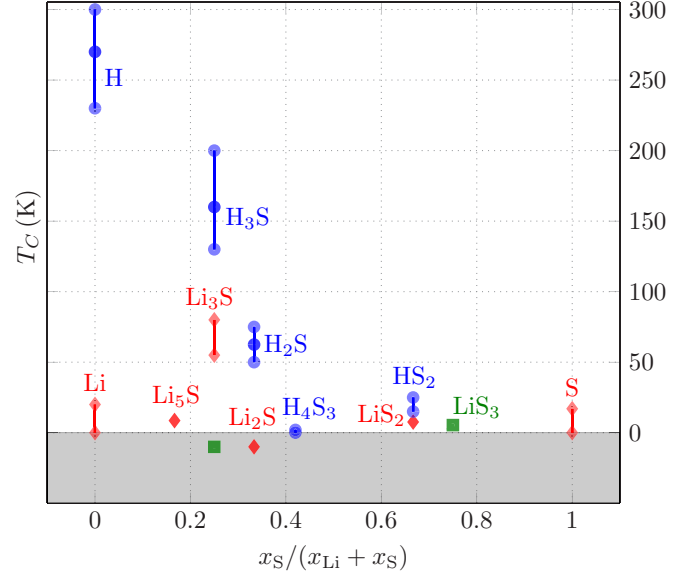


FIG. 3. Calculated  $T_c$ 's of intermediate (green) and high (red) pressure Li-S phases. Blue symbols indicate values for the H-S system, taken from literature [59,60]. The error bars show the variations of  $T_c$  due to pressure, when available. Phases with no superconductivity are shown as negative values.

The calculated values of  $T_c$  are plotted in Fig. 3 as green (100 GPa) and red (500 GPa) symbols. Literature values for different sulfur hydrides from Ref. [59] are shown as blue symbols on the same scale; the error bars indicate pressure variations of  $T_c$ , when known. To give a visual impression of the presence or absence of superconductivity,  $T_c$ 's smaller than 0.5 K are shown as negative. Table I reports the corresponding values of  $\omega_{\log}$  and  $\lambda$ . Since we could not find any literature values, we calculated also data for the  $P4_132$  phase of Li at 500 GPa.

Figure 3 shows that only a few Li-S phases display a finite  $T_c$ , and a single phase, i.e., the high-pressure  $fcc$  phase of  $\text{Li}_3\text{S}$ , displays a critical temperature comparable to that of

TABLE I. Superconducting properties of the metallic Li-S phases.  $T_c$ 's are estimated from Eq. (1), with  $\mu^* = 0.1$ . Pressures are in GPa,  $\omega_{\log}$  and  $T_c$ 's are in K;  $\tilde{N}(E_F)$  is the DOS at the Fermi level, in  $\text{st/Ry}$ , divided by the number of atoms in the unit cell;  $\eta = \lambda/\tilde{N}(E_F)$  is in Ry atoms. Data for  $\text{H}_3\text{S}$  are from Ref. [6].

Comp.	$P$	$\omega_{\log}$	$\lambda$	$T_c$	$\tilde{N}(E_F)$	$\eta$
$\text{Li}_3\text{S}$ ( $Pm\bar{3}m$ )	100	754	0.08	0.0	0.62	0.13
$\text{LiS}_3$ ( $Im\bar{3}m$ )	100	409	0.52	5.4	1.45	0.36
Li ( $P4_132$ )	500	546	0.40	2.2	0.25	1.64
$\text{Li}_5\text{S}$ ( $Immm$ )	500	420	0.53	8.6	0.48	1.10
$\text{Li}_3\text{S}$ ( $Pm\bar{3}m$ )	500	702	0.25	0.0	0.67	0.37
$\text{Li}_3\text{S}$ ( $Fm\bar{3}m$ )	500	773	1.43	80.0	1.67	0.85
$\text{Li}_3\text{S}$ ( $Fm\bar{3}m$ )	640	842	0.90	50.1	1.20	0.75
$\text{Li}_3\text{S}$ ( $P6_3/mmc$ )	500	374	0.22	0.0	0.27	0.85
$\text{LiS}_2$ ( $I4/mmm$ )	500	494	0.54	7.6	1.35	0.40
$\text{H}_3\text{S}$ ( $Im\bar{3}m$ )	200	1200	2.40	180	1.83	1.31
$\text{Li}_3\text{S}^{\text{H}}$ ( $Fm\bar{3}m$ )	500	1156	1.43	169	1.67	0.86

hydrides. Furthermore, two of the phases with a finite  $T_C$ ,  $\text{Li}_3\text{S}$  and  $\text{Li}_2\text{S}$ , are S-rich phases, in which the  $ep$  coupling is dominated by the sulfur sublattice, and thus not directly related to hydrides. Other Li-rich phases, including elemental Li, exhibit  $T_C$ 's lower than 20 K. The contrast with the corresponding hydrides is striking: for some compositions the differences in  $T_C$  are as large as two orders of magnitude. This suggests a fundamental difference between hydrogen- and lithium-rich compounds, which we will investigate based on Eq. (1) and Table I.

First, the higher atomic mass of lithium implies a smaller prefactor  $\omega_{\log}$  in Eq. (1). To a first approximation, the reduction can be estimated as  $\sqrt{M_{\text{Li}}/M_{\text{H}}} \simeq 2.6$ . For most cases reported in Table I, this is clearly not the dominating effect. The single notable exception is  $Fm\bar{3}m\text{-Li}_3\text{S}$ , which is the only truly high- $T_C$  phase identified in our study; its  $T_C$  is 80 K at 500 GPa, where it is metastable, and decreases to 50 K in its stability range. If we take into account the mass effect, the  $T_C$  is comparable to that of  $\text{H}_3\text{S}$ . To prove that, we performed a calculation in which we replaced the Li mass with that of hydrogen; this phase is indicated as  $\text{Li}_3\text{S}^{\text{H}}$  in the table. The calculated  $T_C$  is 170 K, i.e., comparable to that of  $\text{H}_3\text{S}$ . We want to note, however, that the pressure needed to stabilize a high- $T_C$  phase in this case is almost three times larger as in the hydrides. We will discuss this point further in the following.

Table I shows that with the exception of  $Fm\bar{3}m\text{-Li}_3\text{S}$ , where  $\lambda \geq 1$ , all Li-S phases have small or at best intermediate  $ep$  coupling constants ( $0.1 < \lambda < 0.55$ ). The simplified Hopfield expression  $\lambda = \frac{N(E_F)I^2}{M\omega^2}$ , where  $I$  is an average  $ep$  matrix element and  $M\omega^2$  is an average lattice force constant, permits us to separate the  $ep$  coupling into a purely electronic contribution given by the DOS and a factor  $\eta = \frac{I^2}{M\omega^2}$  related to the lattice. Values of  $\tilde{N}(E_F)$ , i.e., DOS per atom, and  $\eta$  for all Li-S phases in Fig. 3 are reported in Table I.

First of all, we notice that in three high-pressure phases, simple cubic Li,  $\text{Li}_5\text{S}$ , and  $\text{Li}_2\text{S}$ ,  $\lambda$  is suppressed by an extremely low  $\tilde{N}(E_F)$ . For Li and  $\text{Li}_5\text{S}$ , the poor metallic behavior is a consequence of  $2s\text{-}2p$  hybridization;  $\text{Li}_2\text{S}$  is instead a semiconducting phase which has been metallized by band overlap, and its DOS is intrinsically low. In the two sulfur-rich phases— $\text{Li}_2\text{S}$  and  $\text{Li}_3\text{S}$ —the  $ep$  coupling is moderate ( $\lambda \sim 0.55$ ) and the DOS is sizable; due to the high sulfur content the characteristic phonon frequencies and  $T_C$ 's are relatively low.

Interestingly, for  $\text{Li}_3\text{S}$  we observe a striking difference between the simple cubic ( $sc$ )  $Pm\bar{3}m$  low- $P$  and the  $fcc$   $Fm\bar{3}m$  high- $P$  structures: The  $sc$  phase has an extremely low  $\lambda = 0.08$  in its stability range, which increases slightly at 500 GPa ( $\lambda = 0.25$ ), where it is still dynamically stable; both values yield negligible  $T_C$ 's. The high- $T_C$   $fcc$  phase, instead, exhibits a very high coupling ( $\lambda = 1.43$ ) at 500 GPa and  $\lambda = 0.90$  at higher pressures (640 GPa); the corresponding  $T_C$ 's are large.

Table I shows that in this case, besides the DOS, there is a remarkable difference in the lattice contribution to the  $ep$  coupling  $\eta$  between the low- and high-pressure phases. This is due to the different nature of electronic states involved in the superconducting pairing in the two structures. In fact, the double- $\delta$  integral in Eq. (2) implies that the only electronic states which give a finite contribution to the  $ep$  coupling are

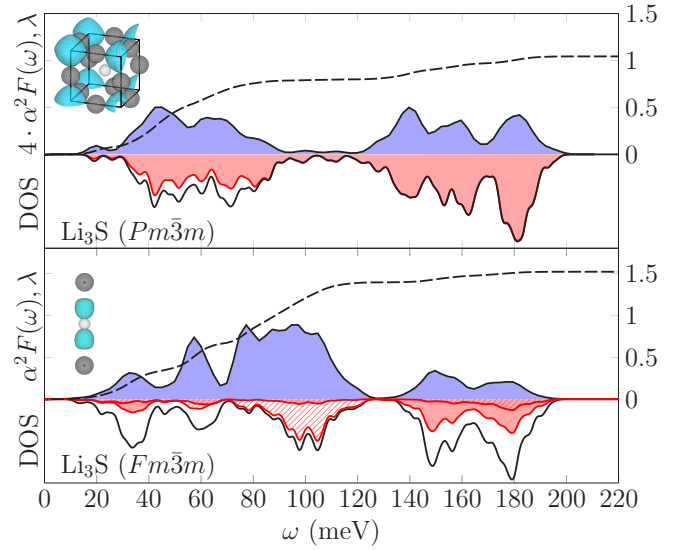


FIG. 4. Above:  $\alpha^2 F(\omega)$  for  $Pm\bar{3}m\text{-Li}_3\text{S}$  (top) and  $Fm\bar{3}m\text{-Li}_3\text{S}$  (bottom) at 500 GPa; the black dashed lines show the frequency-integrated  $ep$  coupling  $\lambda(\omega)$ . Note that the data for  $Pm\bar{3}m\text{-Li}_3\text{S}$  are multiplied by 4. Below: Phonon DOS's. Partial lithium contributions are shown in red; the dashed areas in  $Fm\bar{3}m\text{-Li}_3\text{S}$  indicate vibrations of the Li atoms which form bonds with S in the (100) direction (red dashed lines in Fig. 2). The insets show isocontours of the square of the wave function for the electronic bands that cross the Fermi level.

those that are at  $E_F$ . If these states have a large intrinsic coupling to phonons, as in covalently bonded solids,  $\eta$  and thus  $\lambda$  are large [4,5,61]. On the contrary, interstitial electrons, which are localized in empty regions of the crystal structure, couple very little to lattice vibrations, and hence  $\eta$  and  $\lambda$  will be low.

Figure 4 illustrates how the superconducting properties of  $Pm\bar{3}m\text{-}$  and  $Fm\bar{3}m\text{-Li}_3\text{S}$  differ due to matrix elements effects. The two main panels show the Eliashberg spectral functions and partial phonon DOS's calculated for both phases at 500 GPa: the two spectra extend up to 180 meV, but the intensity and spectral distribution of the  $ep$  coupling is crucially different. Note that for better readability of the figure,  $\alpha^2 F(\omega)$  and  $\lambda$  of  $Pm\bar{3}m\text{-Li}_3\text{S}$  are multiplied by 4.  $Pm\bar{3}m\text{-Li}_3\text{S}$  has an extremely uniform (and low)  $ep$  coupling, while  $Fm\bar{3}m\text{-Li}_3\text{S}$  shows a strong enhancement in the spectral region which corresponds to modes that distort the long Li-S bonds in the (100) direction. In the small insets we plot isocontours of the square of the wave functions for the electronic states at the Fermi level; see the SM for the definition [55]. In  $Pm\bar{3}m\text{-Li}_3\text{S}$ , these are localized in the interstitial region, i.e., around the corners of the cube. In  $Fm\bar{3}m\text{-Li}_3\text{S}$ , on the other hand, they are localized along the edges of the cube, i.e., along the long (100) Li-S bonds, indicated by the red dashed lines in Fig. 2. The different nature of the electronic states leads to a factor of  $\sim 3$  increase in  $\eta$ ; the difference in  $\lambda$  is even larger.

We thus find that interstitial charge localization due to avoided core overlap can be a fundamental limiting factor for conventional superconductivity. This feature is very common in many alkali-metal-rich phases, including several new Li-S phases of this study, indicated by dashed areas in Fig. 1. When, as in  $Pm\bar{3}m\text{-Li}_3\text{S}$ , the electron count is such that interstitial

charge localization involves electrons at  $E_F$ , the  $ep$  coupling is strongly suppressed.

In conclusion, in this work we studied the thermodynamic stability and superconducting properties of the Li-S system up to 700 GPa, using methods for *ab initio* crystal structure prediction and linear response calculations of the  $ep$  coupling. The calculated convex hulls show that several compositions besides the ambient pressure  $\text{Li}_2\text{S}$  are stabilized with increasing pressure. Most of these phases are metallic, but they exhibit no or low- $T_C$  superconductivity. We attribute this to two detrimental effects of core electrons in lithium: (i) an increased insulating behavior under pressure due to hybridization between  $2s$  and  $2p$  electronic states; and (ii) interstitial charge localization due to avoided core overlap, which can bring states to the Fermi level that are intrinsically not coupled to lattice vibrations. This is observed for example

in  $\text{Li}_3\text{S}$ , where a high- $T_C$  *fcc* phase appears only at pressures high enough to stabilize close-packed structures. For this phase we predict a  $T_C$  of 50 K at 640 GPa, where it is the ground-state structure, which increases up to 80 K at 500 GPa, where it could be stabilized as a metastable phase [14]. Note that the phase boundaries predicted in our study could also be shifted due to anharmonic effects, as seen in hydrides [62].

Our study thus shows that high- $T_C$  superconductivity at megabar pressures can be attained in Li-rich compounds, similar to hydrides, but a general tendency to insulating behavior and avoided core overlap will limit the possible range of pressures and dopings.

The authors acknowledge computational resources from the *dCluster* of the Graz University of Technology and the VSC3 of the Vienna University of Technology.

- 
- [1] A. P. Drozdov, M. I. Eremets, I. A. Troyan, V. Knenfontov, and S. I. Shylin, *Nature* **525**, 73 (2015).
- [2] I. Troyan, A. Gavriluk, R. Ruffer, A. Chumakov, A. Mironovich, I. Lyubutin, D. Perekalin, A. P. Drozdov, and M. I. Eremets, *Science* **351**, 1303 (2016).
- [3] D. Duan, Y. Liu, F. Tian, D. Li, X. Huang, Z. Zhao, H. Yu, B. Liu, W. Tian, and T. Cui, *Sci. Rep.* **4**, 6968 (2014).
- [4] N. Bernstein, C. S. Hellberg, M. D. Johannes, I. I. Mazin, and M. J. Mehl, *Phys. Rev. B* **91**, 060511 (2015).
- [5] C. Heil and L. Boeri, *Phys. Rev. B* **92**, 060508 (2015).
- [6] J. A. Flores-Livas, A. Sanna, and E. K. U. Gross, *Eur. Phys. J. B* **89**, 63 (2016).
- [7] Y. Quan and W. E. Pickett, *Phys. Rev. B* **93**, 104526 (2016).
- [8] Y. Li, J. Hao, H. Liu, Y. Li, and Y. Ma, *J. Chem. Phys.* **140**, 174712 (2014).
- [9] D. A. Papaconstantopoulos, B. M. Klein, M. J. Mehl, and W. E. Pickett, *Phys. Rev. B* **91**, 184511 (2015).
- [10] L. Ortenzi, E. Cappelluti, and L. Pietronero, *arXiv:1511.04304*.
- [11] I. Errea, M. Calandra, C. J. Pickard, J. Nelson, R. J. Needs, Y. Li, H. Liu, Y. Zhang, Y. Ma, and F. Mauri, *Phys. Rev. Lett.* **114**, 157004 (2015).
- [12] A. Drozdov, M. I. Eremets, and I. A. Troyan, *arXiv:1508.06224*.
- [13] A. Shamp, T. Terpstra, T. Bi, Z. Falls, P. Avery, and E. Zurek, *J. Am. Chem. Soc.* **138**, 1884 (2016).
- [14] J. A. Flores-Livas, M. Amsler, C. Heil, A. Sanna, L. Boeri, G. Profeta, C. Wolverton, S. Goedecker, and E. K. U. Gross, *Phys. Rev. B* **93**, 020508 (2016).
- [15] Y. Fu, X. Du, L. Zhang, F. Peng, M. Zhang, C. J. Pickard, R. J. Needs, D. J. Singh, W. Zheng, and Y. Ma, *Chem. Mater.* **28**, 1746 (2016).
- [16] N. Ashcroft, *Phys. Rev. Lett.* **21**, 1748 (1968).
- [17] P. Cudazzo, G. Profeta, A. Sanna, A. Floris, A. Continenza, S. Massidda, and E. K. U. Gross, *Phys. Rev. Lett.* **100**, 257001 (2008).
- [18] J. M. McMahon and D. M. Ceperley, *Phys. Rev. B* **84**, 144515 (2011).
- [19] M. Borinaga, I. Errea, M. Calandra, F. Mauri, and A. Bergara, *Phys. Rev. B* **93**, 174308 (2016).
- [20] R. Szczeniak and M. Jarosik, *Solid State Commun.* **149**, 2053 (2009).
- [21] M. I. Eremets, I. A. Troyan, and A. P. Drozdov, *arXiv:1601.04479*.
- [22] P. Dalladay-Simpson, R. T. Howie, and E. Gregoryanz, *Nature* **529**, 63 (2016).
- [23] N. W. Ashcroft, *Phys. Rev. Lett.* **92**, 187002 (2004).
- [24] J. S. Tse, Y. Yao, and K. Tanaka, *Phys. Rev. Lett.* **98**, 117004 (2007).
- [25] G. Gao, A. R. Oganov, P. Li, Z. Li, H. Wang, T. Cui, Y. Ma, A. Bergara, A. O. Lyakhov, T. Iitaka, and G. Zou, *Proc. Natl. Acad. Sci. USA* **107**, 1317 (2010).
- [26] D. Y. Kim, R. H. Scheicher, H.-k. Mao, T. W. Kang, and R. Ahuja, *Proc. Natl. Acad. Sci. USA* **107**, 2793 (2010).
- [27] Y. Yao and D. D. Klug, *Proc. Natl. Acad. Sci. USA* **107**, 20893 (2010).
- [28] J. A. Flores-Livas, M. Amsler, T. J. Lenosky, L. Lehtovaara, S. Botti, M. A. L. Marques, and S. Goedecker, *Phys. Rev. Lett.* **108**, 117004 (2012).
- [29] A. Oganov *et al.*, USPEX code, available at <http://uspex.stonybrooke.edu>.
- [30] For selected phases we calculated the  $ep$  properties using DFPT, as implemented in QUANTUM ESPRESSO [31]. We employed PBE ultrasoft pseudopotentials with semicore states in valence for lithium and sulfur from the standard QUANTUM ESPRESSO distribution, with energy cutoffs of 80 and 800 Ry for wave functions and charge density, respectively. We used  $8^3\mathbf{k}$ - and  $\mathbf{q}$ -point meshes for reciprocal space integration for electron and phonon states in the self-consistent calculations, and up to  $38^3\mathbf{k}$  points for the  $ep$  matrix elements.
- [31] P. Giannozzi, S. Baroni, N. Bonini, M. Calandra, R. Car, C. Cavazzoni, D. Ceresoli, G. L. Chiarotti, M. Cococcioni, I. Dabo, A. Dal Corso, S. de Gironcoli, S. Fabris, G. Fratesi, R. Gebauer, U. Gerstmann, C. Gougoussis, A. Kokalj, M. Lazzeri, L. Martin-Samos, N. Marzari, F. Mauri, R. Mazzarello, S. Paolini, A. Pasquarello, L. Paulatto, C. Sbraccia, S. Scandolo, G. Sclauzero, A. P. Seitsonen, A. Smogunov, P. Umari, and R. M. Wentzcovitch, *J. Phys. Condens. Matter* **21**, 395502 (2009).
- [32] A. Grzechnik, A. Vegas, K. Syassen, I. Loa, M. Hanfland, and M. Jansen, *J. Solid State Chem.* **154**, 603 (2000).
- [33] A. Lazicki, C.-S. Yoo, W. J. Evans, and W. E. Pickett, *Phys. Rev. B* **73**, 184120 (2006).

- [34] I. I. Naumov, R. J. Hemley, R. Hoffmann, and N. Ashcroft, *J. Chem. Phys.* **143**, 064702 (2015).
- [35] M. Hanfland, K. Syassen, N. Christensen, and D. Novikov, *Nature* **408**, 174 (2000).
- [36] L. Shi and D. A. Papaconstantopoulos, *Phys. Rev. B* **73**, 184516 (2006).
- [37] N. E. Christensen and D. L. Novikov, *Phys. Rev. B* **73**, 224508 (2006).
- [38] M. Marqués, M. I. McMahon, E. Gregoryanz, M. Hanfland, C. L. Guillaume, C. J. Pickard, G. J. Ackland, and R. J. Nelmes, *Phys. Rev. Lett.* **106**, 095502 (2011).
- [39] B. Rousseau and N. W. Ashcroft, *Phys. Rev. Lett.* **101**, 046407 (2008).
- [40] M. Marqués, G. J. Ackland, L. F. Lundegaard, G. Stinton, R. J. Nelmes, M. I. McMahon, and J. Contreras-García, *Phys. Rev. Lett.* **103**, 115501 (2009).
- [41] M. Gatti, I. V. Tokatly, and A. Rubio, *Phys. Rev. Lett.* **104**, 216404 (2010).
- [42] Y. Xie, A. R. Oganov, and Y. Ma, *Phys. Rev. Lett.* **104**, 177005 (2010).
- [43] C. J. Pickard and R. J. Needs, *Nat. Phys.* **3**, 473 (2007).
- [44] Y. Yao, J. S. Tse, K. Tanaka, F. Marsiglio, and Y. Ma, *Phys. Rev. B* **79**, 054524 (2009).
- [45] G. Profeta, C. Franchini, N. N. Lathiotakis, A. Floris, A. Sanna, M. A. L. Marques, M. Lüders, S. Massidda, E. K. U. Gross, and A. Continenza, *Phys. Rev. Lett.* **96**, 047003 (2006).
- [46] F. Murnaghan, *Proc. Natl. Acad. Sci. USA* **30**, 244 (1944).
- [47] We explored the Li-S system using the technique of *ab initio* evolutionary crystal structure prediction as implemented in the USPEX package [50,63,64]. The underlying structural relaxations were performed using the VASP code, [65,66] within the generalized gradient approximation [67]. We used the all-electron projector-augmented wave method [68,69]. To avoid core overlap at high pressures in Li, we treated the 1s and 2s electrons as valence. Individual structures generated by the evolutionary algorithms were relaxed with increasing precision in a five-step procedure; the energies were finally recalculated with increasing convergence criteria to ensure a correct ranking of the structure.
- [48] For all evolutionary runs, we limited trapping in local minima by repeating simulations at selected pressures and using the antiseeds-technique described in Ref. [29]. To ensure a reliable ranking of the structures, we performed extensive convergence checks of the total energy and forces with respect to cutoff energy and  $\mathbf{k}$ -point resolution; for variable and fixed composition runs we used energy cutoffs up to 700–800 eV, and a  $\mathbf{k}$ -point resolution of  $0.06\ 2\pi/\text{\AA}$  to obtain a first rough approximation of the enthalpies; for the final enthalpy vs pressure curves, we increased these values up to 1100 to 1200 eV and Monkhorst-Pack  $\mathbf{k}$ -point meshes for sampling the Brillouin zone with resolution of  $0.03\ 2\pi/\text{\AA}$ , which ensured a convergence of forces up to 1 meV/atom.
- [49] Y. Ma, A. R. Oganov, and Y. Xie, *Phys. Rev. B* **78**, 014102 (2008).
- [50] A. R. Oganov and C. W. Glass, *J. Chem. Phys.* **124**, 244704 (2006).
- [51] O. Zakharov and M. L. Cohen, *Phys. Rev. B* **52**, 12572 (1995).
- [52] O. Degtyareva, E. Gregoryanz, M. Somayazulu, H.-k. Mao, and R. J. Hemley, *Phys. Rev. B* **71**, 214104 (2005).
- [53] A. Vegas, A. Grzechnik, K. Syassen, I. Loa, M. Hanfland, and M. Jansen, *Acta Crystallogr. Sect. B* **57**, 151 (2001).
- [54] A. Vegas, A. Grzechnik, M. Hanfland, C. Mühle, and M. Jansen, *Solid State Sci.* **4**, 1077 (2002).
- [55] See Supplemental Material at <http://link.aps.org/supplemental/10.1103/PhysRevB.94.060502> for details of the crystal structures, electronic band structures and DFPT results for all phases considered in this study.
- [56] A. Lazicki, B. Maddox, W. J. Evans, C.-S. Yoo, A. K. McMahan, W. E. Pickett, R. T. Scalettar, M. Y. Hu, and P. Chow, *Phys. Rev. Lett.* **95**, 165503 (2005).
- [57] J. P. Carbotte, *Rev. Mod. Phys.* **62**, 1027 (1990).
- [58] P. B. Allen and B. Mitrović, *Theory of Superconducting Tc*, Vol. 37 (Academic, New York, 1983), pp. 1–92.
- [59] Y. Li, L. Wang, H. Liu, Y. Zhang, J. Hao, C. J. Pickard, J. R. Nelson, R. J. Needs, W. Li, Y. Huang, I. Errea, M. Calandra, F. Mauri, and Y. Ma, *Phys. Rev. B* **93**, 020103 (2016).
- [60] R. Akashi, W. Sano, R. Arita, and S. Tsuneyuki, [arXiv:1512.06680](https://arxiv.org/abs/1512.06680).
- [61] L. Boeri, J. Kortus, and O. K. Andersen, *Phys. Rev. Lett.* **93**, 237002 (2004).
- [62] I. Errea, M. Calandra, C. J. Pickard, J. R. Nelson, R. J. Needs, Y. Li, H. Liu, Y. Zhang, Y. Ma, and F. Mauri, *Nature* **532**, 81 (2016).
- [63] A. O. Lyakhov, A. R. Oganov, H. T. Stokes, and Q. Zhu, *Comput. Phys. Commun.* **184**, 1172 (2013).
- [64] A. R. Oganov, A. O. Lyakhov, and M. Valle, *Acc. Chem. Res.* **44**, 227 (2011).
- [65] G. Kresse and J. Hafner, *Phys. Rev. B* **47**, 558 (1993).
- [66] G. Kresse and J. Furthmüller, *Comput. Mater. Sci.* **6**, 15 (1996).
- [67] J. P. Perdew, K. Burke, and M. Ernzerhof, *Phys. Rev. Lett.* **77**, 3865 (1996).
- [68] G. Kresse and D. Joubert, *Phys. Rev. B* **59**, 1758 (1999).
- [69] P. E. Blöchl, *Phys. Rev. B* **50**, 17953 (1994).